Journal of Power Sources 189 (2009) 806–808

Contents lists available at ScienceDirect

Journal of Power Sources

journal homepage: www.elsevier.com/locate/jpowsour

Short communication

Atomic-scale characterization of tin-based intermetallic anodes

S. Naille [a], R. Dedryvère [b], D. Zitoun [a], P.-E. Lippens [a,*]

[a] ICG/AIME, CNRS UMR 5253, Université-Montpellier II, CC1502 Place E. Bataillon, 34095 Montpellier Cedex 5, France
[b] IPREM/ECP, CNRS UMR, Université de Pau et des Pays de l'Adour, Hélioparc Pau-Pyrénées, 2 av. Pierre Angot, 64053 Pau Cedex 9, France

ARTICLE INFO

Article history:
Received 27 June 2008
Accepted 21 July 2008
Available online 29 July 2008

Keywords:
Tin
Anodes
Mössbauer spectroscopy
X-ray photoelectron spectroscopy
Superparamagnetism
Nanoparticles

ABSTRACT

Electrochemical reactions of lithium with Ni_3Sn_4- and $CoSn_2$-based anodes for Li-ion batteries are analysed from a combined experimental and theoretical approach. We have found that the first discharge consists in the nanostructuration of the pristine materials into metallic and Li_7Sn_2 nanoparticles. Then, the basic mechanism of the charge and discharge cycles is the reversible transformation of Li_7Sn_2 into Ni_3Sn_4 or $CoSn_2$ particles. Finally, the large irreversible capacity loss observed at the beginning of the first discharge is explained from interfacial reactions.

1. Introduction

Improvements in the electrochemical performances of Li-ion batteries require the development of new electrode materials with high capacities. Recently, there has been substantial interest in tin-based intermetallic materials in order to replace carbon as negative electrode [1–3]. For example, Sony has commercialized a Li-ion battery, named Nexelion™, with a composite anode formed of tin, cobalt and carbon mixed at a nanometer level, inducing a 30% increase in capacity per volume ratio [4]. The ability to effectively engineer these new materials requires a detailed understanding of the mechanisms that occur during the charge and the discharge cycles. In most cases, studies are based on X-ray diffraction that unfortunately fails to characterize nanocrystalline or amorphous phases formed during electrochemical reactions.

In the present study, we propose to combine X-ray diffraction, Mössbauer spectroscopy, X-ray photoemission spectroscopy (XPS), magnetic measurements and calculations based on density functional theory (DFT) in order to understand the reactions between lithium and tin based intermetallic anodes at the atomic scale.

2. Experimental

The intermetallic compounds Ni_3Sn_4 and $CoSn_2$ were synthesized directly from pure elements, weighed in stoichiometric ratio, in alumina crucibles under a controlled Ar/H_2 (5%) atmosphere. Temperature programs were 4 h at 500 °C for Ni_3Sn_4 and 5 h at 500 °C for $CoSn_2$.

Electrochemical lithium insertion/extraction tests were carried out with (Li/$LiPF_6$ 1 M (EC:PC:3DMC)/material) Swagelok™-type two-electrode cells assembled inside an argon-filled glove box. Cathodes were prepared as 7-mm diameter pellets by pressing a mixture made up of 80 wt.% pristine materials, 10 wt.% PTFE binder, and 10 wt.% carbon black to improve the mechanical and electronic conduction properties. Electrochemical discharge/charge curves were recorded on a multichannel Mac Pile II system under galvanostatic conditions at a rate of 1 Li/20 h (C/20).

X-ray diffraction (XRD) was performed, for phase identification and purity, with a Philips θ–2θ diffractometer using Cu Kα radiation (λ = 1.5418 Å) and a nickel filter. Data gathering were performed in continuous mode for 2θ angles ranging from 10° to 70°. The powdered sample was observed by scanning electron microscopy (SEM) in order to characterize both the sample morphology and the particle size.

XPS measurements were carried out with a Kratos Axis Ultra spectrometer using a focused monochromatized Al Kα radiation ($h\nu$ = 1486.6 eV). For the Ag $3d_{5/2}$ line the full width at half maximum (FWHM) was 0.58 eV under the recording conditions. The binding energy scale was calibrated from the carbon contamination using the C 1s peak at 285.0 eV. Core peaks were analyzed using a nonlinear Shirley-type background [5]. The peak positions and areas were optimized by a weighted least-square fitting method using 70% Gaussian, 30% Lorentzian lineshapes. Quantification was performed on the basis of Scofield's relative sensitivity factors [6].

* Corresponding author. Tel.: +33 4 67144548; fax: +33 4 67143304.
E-mail address: lippens@univ-montp2.fr (P.-E. Lippens).

0378-7753/$ – see front matter © 2008 Elsevier B.V. All rights reserved.
doi:10.1016/j.jpowsour.2008.07.049

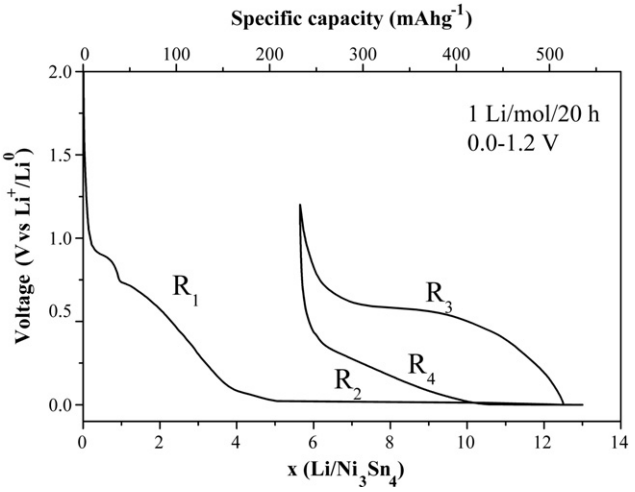

Fig. 1. Voltage profile of Ni_3Sn_4 electrode. Regions R_1–R_4 are considered for the analysis of the mechanisms.

The ^{119}Sn Mössbauer spectra were recorded in transmission mode in the constant acceleration mode. The source used for experiments was ^{119m}Sn embedded in a $CaSnO_3$ matrix. The velocity scale was calibrated with the magnetic sextet of a high purity iron foil as the reference absorber, and ^{57}Co (Rh) was used as the source. The spectra were fit to Lorentzian profiles by the non-linear-least-square method with the G.M.5.S.I.T. program [7] and the quality of the fits were controlled by the usual χ^2 test. The isomer shifts are given relative to $BaSnO_3$ at room temperature which is used as the standard reference.

Magnetic properties were measured using a Superconducting Quantum Interference Design (SQUID) magnetometer MPMS XL7, in the range of temperature 2–300 K and field 0–5 T. The temperature-dependent susceptibility was measured using DC procedure. The sample was dried in a glovebox and transferred under argon to the SQUID chamber to prevent any oxidation. The sample was cooled to 2.0 K under zero magnetic field, low magnetic field (0.05 T) was applied and data collected from 2 K to 300 K (zero-field cooled, ZFC). Field cooled (FC) measurements were performed from 2 K to 300 K with an applied field during the cooling.

3. Result and discussion

The voltage profiles obtained in galvanostatic modes (C/20) are very similar for Ni_3Sn_4 and $CoSn_2$ and we have defined four regions corresponding to the first discharge: voltage drop R_1 followed by a plateau R_2, the first charge R_3 and the second discharge R_4 (Fig. 1). The voltage profile of the following cycles is similar to R_3 and R_4 except for a decrease in the capacity.

For both Ni_3Sn_4 and $CoSn_2$ the voltage promptly drops to about 0.8 V in the region R_1 with a small plateau which indicates the formation of a surface electrode interphase (SEI) at the carbonated additive surface. Then, the voltage continuously decreases until the appearance of a plateau at a voltage close to 0.1 V for about 1–2 Li for $CoSn_2$ and 2–4 Li for Ni_3Sn_4. No change was observed from the different experimental techniques including DRX, which indicates that the pristine materials did not react with lithium in this region. Only XPS shows the formation of a layer mainly composed by Li_2CO_3 and LiF at the surface of the intermetallic particles (Fig. 2). The average thickness of this layer increases in this region during the lithiation and then remains almost constant in the other regions R_2–R_4. This clearly indicates that lithium ions react with electrolyte at the surface of the intermetallic particles and form a SEI in R_1 [8].

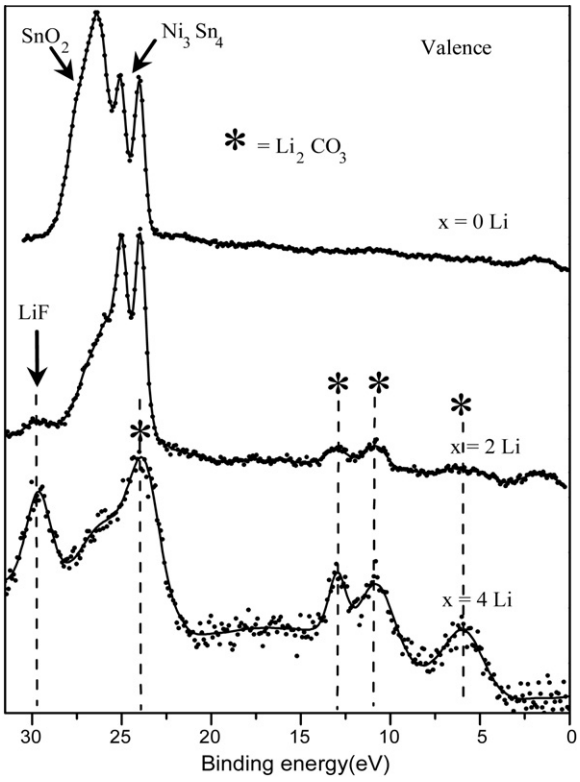

Fig. 2. XPS valence bands of Ni_3Sn_4 electrode at different steps in R_1.

The region R_2 concerns a plateau at very low potential. X-ray diffraction shows that contribution of Ni_3Sn_4 (or $CoSn_2$) decreases and a new phase occurs. The latter phase cannot be determined from this technique although the observed diffraction peaks are in

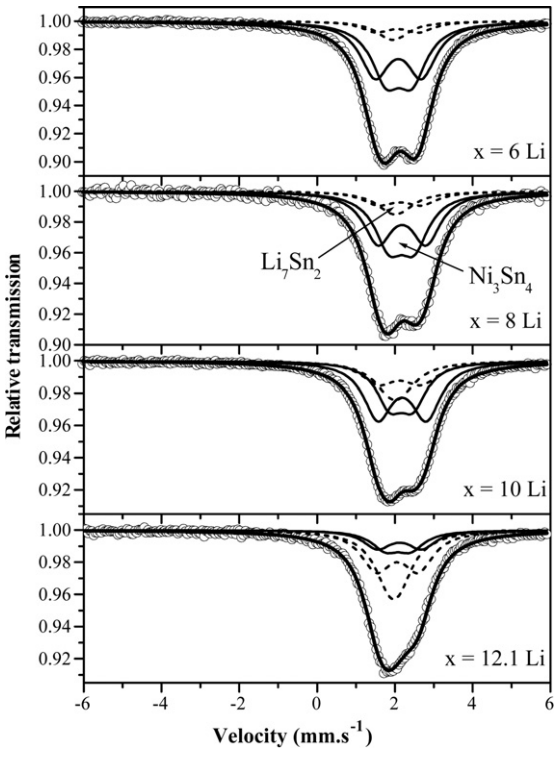

Fig. 3. ^{119}Sn Mössbauer spectra at room temperature of Ni_3Sn_4 electrode at different steps in R_2.

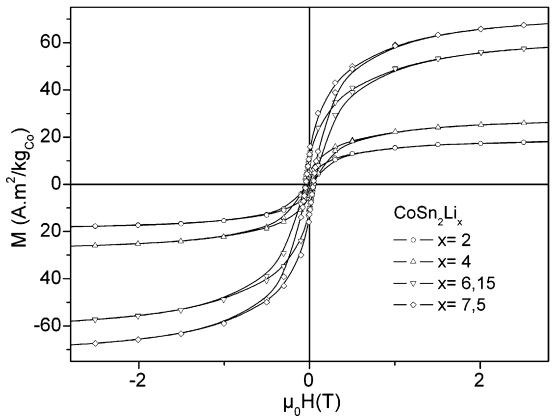

Fig. 4. Magnetic measurements at $T = 2$ K of $CoSn_2$-based electrode at different steps in R_2.

the range of the Li-rich Li_xSn compounds. However, the composition Li_7Sn_2 has been unambiguously determined from both *in situ* and *ex situ* ^{119}Sn Mössbauer spectroscopy from the comparison with reference spectra [9] (Fig. 3).

Thus, the region R_2 can be assigned to the displacement reactions:

$$Ni_3Sn_4 + 14Li \rightarrow 2Li_7Sn_2 + 3Ni \quad (1)$$

$$CoSn_2 + 7Li \rightarrow Li_7Sn_2 + Co \quad (2)$$

In addition it is possible from the knowledge of the Lamb–Mössbauer factors to evaluate the amounts of the different species and to quantitatively follow the reactions [10]. The proposed reactions (1) and (2) differ from the usual mechanism found in the literature that indicates the formation of $Li_{22}Sn_5$ [11]. Thus, our results show that the expected specific capacities for intermetallic compounds are lower than those reported in the literature. Finally, magnetic measurements show that the average magnetic moment of the electrode material increases during lithiation in R_2 due to the transformation of paramagnetic pristine materials into ferromagnetic Ni (or Co) particles (Fig. 4). ZFC/FC curves (Fig. 5) indicate that the average diameter of the metallic particles is about 6 nm in the case of nickel and 4 nm in the case of cobalt. The average size is constant during the discharge and no exchange interaction is detectable, which confirms that Ni and Co nanoparticles are dispersed and can act as buffer particles to limit volume variations of the electrodes. At the end of the first discharge, the electrode is a composite material

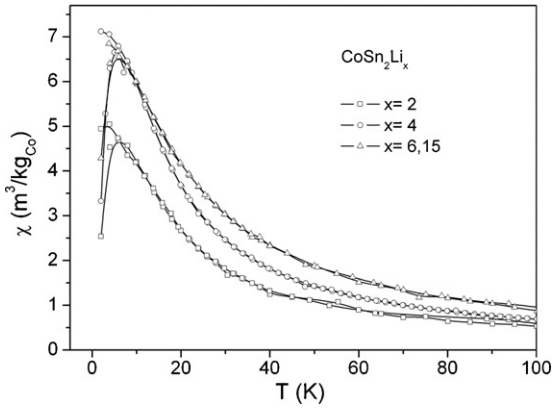

Fig. 5. Susceptibility measurements at $\mu_0 H = 0.05$ T of $CoSn_2$-based electrode at different steps in R_2.

formed by Ni (or Co) nanoparticles and Li_7Sn_2 electrochemically active particles. Thus, the first discharge can be considered as an activation process leading to the formation of a nanocomposite material.

During the first charge (region R_3), Li_7Sn_2 directly reacts with the metallic particles to form Ni_3Sn_4 (or $CoSn_2$) small particles as observed by Mössbauer spectroscopy. In addition, XPS indicates the existence of a Li-poor Li_xSn phase, probably at the surface of the Li_7Sn_2 particles, which was not observed during the discharge. This suggests that delithiation of Li_7Sn_2 leads to the formation of a tin-rich layer at the surface that can react with metal nanoparticles to reform tin-metal compounds with the same composition as the pristine material but with another texture.

Finally, in the second discharge (R_4), the reaction observed by Mössbauer spectroscopy is similar to that of R_2 although the voltage is higher. The theoretical values of the potential obtained from DFT calculations by considering the reactions (1)–(2) are close to the average potentials measured in the regions R_3–R_4. This average potential increases from Ni_3Sn_4 to $CoSn_2$ in agreement with the increase of the calculated cohesive energy of the materials. The very low potential of the plateau in the region R_2 could be related to an additional energy required at the beginning of the first discharge to initiate the displacement reactions (1)–(2). As long as lithium ions cannot react with the pristine materials they irreversibly react with the electrolyte to form a SEI at the particle surface.

4. Conclusion

In conclusion, the electrochemical reactions of lithium with tin intermetallic compounds are initiated at very low voltage. This leads to an irreversible formation of a SEI at both carbon and intermetallic particle surface and causes a loss of 1–4 Li during the first discharge. Then, the pristine material is transformed into Li_7Sn_2, which decreases the reversible capacity expected with $Li_{22}Sn_5$. At the end of the first discharge, a nanocomposite electrode composed by metallic nanoparticles and Li_7Sn_2 is formed and can be considered as the true starting electrode material for the reversible transformation $Ni_3Sn_4/CoSn_2 \leftrightarrow Li_7Sn_2$. The cycleability of the electrode is mainly related to the latter transformation that strongly depends on the texture of the composite electrode while the overall performances also depend on the irreversible formation of the SEI and the composition of Li_xSn that are both intrinsic to the first discharge mechanism.

Acknowledgements

Financial support by the “Région Languedoc-Roussillon”, the ANR (Liban project) and the European Community (ALISTORE Network of Excellence) are gratefully acknowledged.

References

[1] A.D.W. Todd, R.E. Mar, J.R. Dahn, J. Electrochem. Soc. 153 (2006) A1998–A2005.
[2] J. Hassoun, S. Panero, B. Scrosati, J. Power Sources 160 (2006) 1336–1341.
[3] S. Naille, C.M. Ionica-Bousquet, F. Robert, F. Morato, P.-E. Lippens, J. Olivier-Fourcade, J. Power Sources 174 (2007) 1091–1094.
[4] H. Tanizaki, A. Omaru, US Patent 0 053 131 A1 (2004), to Sony Corporation.
[5] D.A. Shirley, Phys. Rev. B 5 (1972) 4709.
[6] J.H. Scofield, J. Electron Spectrosc. Relat. Phenom. 8 (1976) 129.
[7] K. Ruebenbauer, T. Birchall, Hyperfine Interact. 7 (1979) 125–133.
[8] K.K.D. Ehinon, S. Naille, R. Dedryvère, P.-E. Lippens, J.-C. Jumas, D. Gonbeau, Chem. Mater. 20 (2008) 5388–5398.
[9] F. Robert, P.-E. Lippens, J. Olivier-Fourcade, J.-C. Jumas, F. Gillot, M. Morcrette, J.-M. Tarascon, J. Solid-State Chem. 180 (2007) 339–348.
[10] C.-M. Ionica-Bousquet, P.-E. Lippens, L. Aldon, J. Olivier-Fourcade, J.-C. Jumas, Chem. Mater. 18 (2006) 6442–6447.
[11] R. Benedek, M.M. Thackeray, J. Power Sources 110 (2002) 406–411.